A Molecular Donor-Acceptor System to Induce and Visualize Proton Transfer Across Biomolecules

Ramesh Nandi[1,2], Ganga B. Vamisetti[1,3], Samim Sardar[4], Diego Florio[5, 6], Tomasz Pieńko[1], Fabian Glaser[7], Cosimo D'Andrea[4, 5], Giulio Cerullo[5, 6], Franco V. A. Camargo[6] & Nadav Amdursky[1,8*]

[1]Schulich Faculty of Chemistry, Technion Israel Institute of Technology, Haifa, Israel

[2]Physikalisch-Chemisches Institut, Universität Heidelberg, 69120 Heidelberg, Germany

[3]College of Science, Nanjing Agriculture University, Nanjing 210095, China

[4]Center for Nano Science and Technology @PoliMi, Istituto Italiano di Tecnologia, Via Rubattino 81, 20134 Milan, Italy

[5]Dipartimento di Fisica, Politecnico di Milano, Milan 20133, Italy

[6]Istituto di Fotonica e Nanotecnologie-CNR, Piazza L. da Vinci 32, 20133 Milano, Italy

[7]Technion Center for Structural Biology (TCSB), Technion Human Health Initiative (THHI), Technion-Israel Institute of Technology, Haifa, Israel

[8]School of Mathematical and Physical Sciences, University of Sheffield, Sheffield S3 7HF, United Kingdom

[*]Corresponding author. Email: amdursky@technion.ac.il; n.amdursky@sheffield.ac.uk

Abstract: Proton transfer (PT) is at the heart of fundamental natural biochemical reactions, e.g. in bioenergetics, where proteins are the main proton mediators. PT between two specific points requires a change in the proton motive force via alteration of acid-base properties. Nature solved this problem primarily by modulating the protein structure during the PT process. Here, we introduce a light-triggered proton *donor-bridge-acceptor* approach for inducing and visualizing directional PT in biosystems, specifically peptides. To do so, we synthesize unnatural amino acids containing a light-triggered proton *donor* and *acceptor* and place them at the ends of peptide bridges that differ in their amino acid composition while creating a giant ΔpK_a^* gradient between them upon photoexcitation. Ultrafast optical spectroscopies allow for visualization of the PT process across the *donor-bridge-acceptor* system and extraction of the PT kinetics. Our results reveal the importance of side chains, peptide structure, and environment in promoting PT. We show that helical structures can promote PT even with hydrophobic side chains, whereas titratable oxo-amino-acids can promote PT via their side chains even in an aprotic environment. Our strategy for inducing and visualizing the PT process across any desired pathway can be extended to various peptide systems and into proteins, thus opening a new field of research.

Introduction

Proton transfer (PT) is a ubiquitous fundamental biological reaction. Directional PT reactions are commonly mediated by proteins in numerous biological processes, such as in photosynthesis and respiration (*1-3*). Since PT is essentially an acid-base equilibrium, the PT directionality, i.e., the proton motive force (PMF), is commonly modulated by a change in the protein structure during the PT process. To date, the main experimental approach to probe directional PT across biomolecules is to follow the end result of the PT process, which is usually the translocation of protons across a proton channel/pump or an enzymatic process. In some cases, the biomolecular PT process can be initiated with an external cue, such as with a light flash for light-gated proton channels or by depolarizing the membrane for voltage-gated proton channels, which enables following the kinetics of the PT process from start to end (*4*, *5*). The use of point mutations, chemical modifications, and inhibitors, together with the knowledge of the protein structure, has resulted in the understanding of PT pathways within proteins (*6-9*). In mechanistic terms, it is established that the PT pathway is comprised of specific amino acids that can participate in the formation of hydrogen bonds together with networks of water molecules within the protein (*6*, *7*, *10-12*). Nevertheless, the existing experimental approach to studying PT in biomolecules limits our ability to extract a generalized picture of the PT process from a desired point *A* to point *B* and to measure the associated timescales, which are commonly obtained from computational approaches (*13-15*). Here, we overcome this limitation by introducing a versatile *donor-bridge-acceptor* (**D**-B-**A**) system to induce and investigate PT pathways across peptides and proteins in space and time. We reveal the parameters needed for PT across peptides while deciphering the role of the side chain, the structure, and the environment in this process.

Results and discussions

While **D**-B-**A** systems to induce and follow PT across biomolecules are non-existent, their equivalent for electron transfer (ET) has been known for decades (*16-18*). To promote ET, an artificial light-triggered electron donor/acceptor can be introduced to a model system, thus creating a redox potential difference across the biomolecule upon excitation (Fig 1a). An analogous system to promote PT requires a light-triggered alteration in ΔpK_a as the PMF for the PT process between donor (**D**) and acceptor (**A**), bridged by a biomolecule (Fig. 1b). This is the governing mechanism of our new system that is based on molecular photoacids (PAs) and photobases (PBs) as **D** and **A**, respectively. PAs and PBs are capable of excited-state proton transfer or capture, respectively, stemming from a fundamental difference in pK_a values between their electronic ground-state and excited-state (*19-21*). In this study, we chose 7-hydroxycoumarinyl-4-acetic acid (7HC) as the PA **D** and 6-aminoquinoline (6AQ) as the PB **A**, respectively (Fig. 1c), which were designed to have similar excitation energies to initiate the PT process in a controlled manner (*22-24*). Upon excitation, the acid-base properties of PAs and PBs are altered, resulting in a giant excited-state pK_a gap ($\Delta pK_a^* > 11$, see below), which serves as the PMF for the PT across the bridge (Fig. 1c). Here, we synthesized unnatural amino acids (UAAs) containing the PA and PB, thus enabling the use of solid-phase peptide synthesis (SPPS) to incorporate the proton **D** and **A** at desired positions within peptides. For the first exploration of our system, we chose to synthesize peptides that differ in their amino acid composition, comparing the hydrophobic Ala residue to the titratable oxo-amino-acid of Glu.

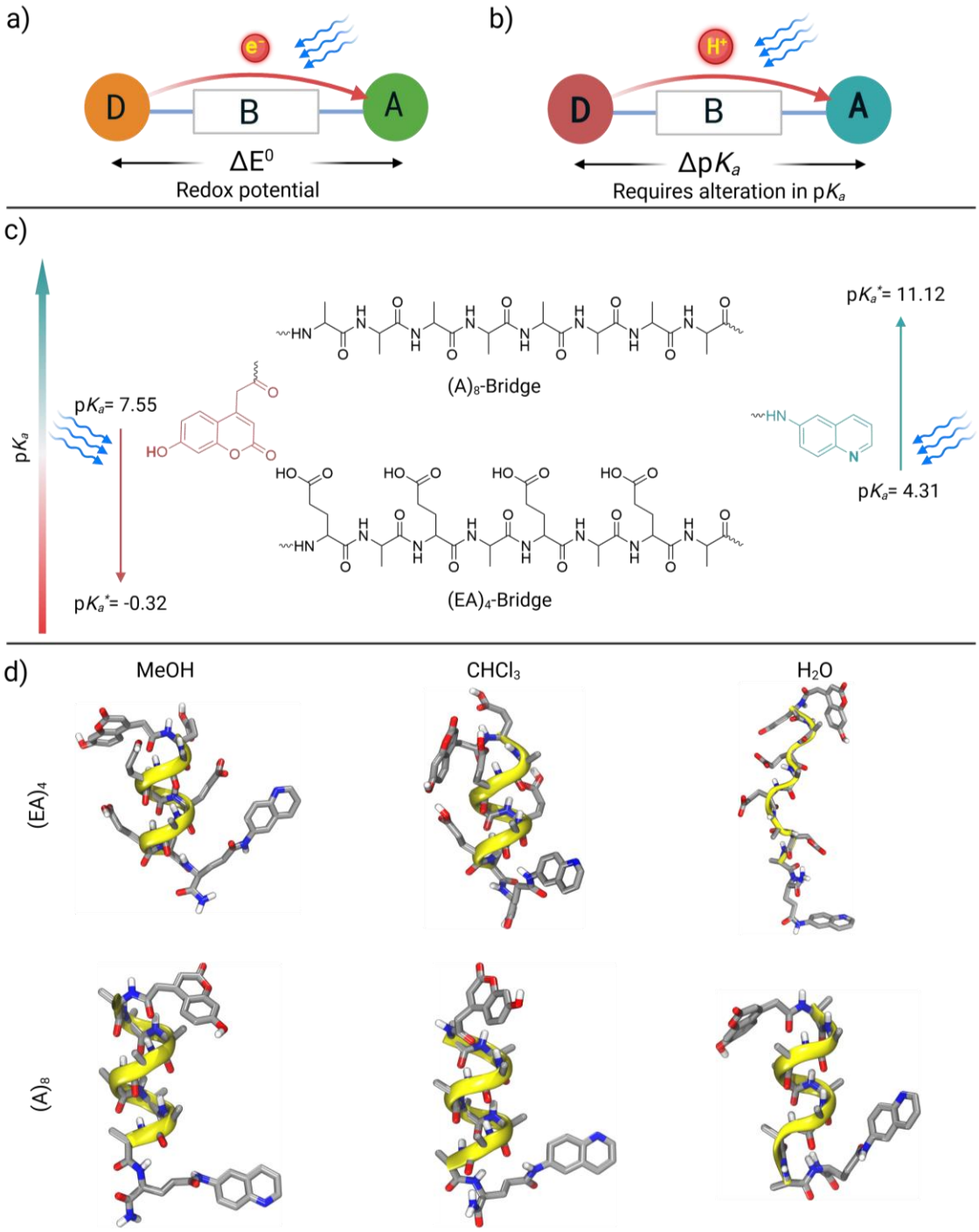

Fig 1: Schematic of light-triggered ET and PT process: a) A schematic of a photo-induced ET process across a bridge between an electron-donor and acceptor. b) The concept of photo-induced PT between a **D** and **A** across a bridge. c) Transient changes in pK_a between ground and excited states in a **D**-B-**A** PT system and the molecular schemes of the **D**, **A**, and bridges used in this study. d) Secondary structure simulations of the different **D**-B-**A** systems in different solvents (MeOH, $CHCl_3$, and H_2O) used in this study.

To synthesize the UAAs, we covalently attached 7HC and 6AQ to the side chain of Fmoc-Lys(OMe)-NH_2 and Fmoc-Glu(OtBu)-COOH, respectively (Schemes S1-4). The final UAA

versions of **D** and **A** are Lys-7HC and Glu-6AQ, respectively (SI section 2). Following the synthesis of the UAAs, the **D**-B-**A** systems were synthesized using SPPS (Schemes S6 and S7). We synthesized two peptide bridges for this study (Fig. 1c): $(Glu\text{-}Ala)_4$ ($(EA)_4$) and Ala_8 ($(A)_8$), both in the presence and absence of the **A**; **D**-B-**A** and **D**-B configurations. As stated, the bridges were chosen based on the involvement of titratable oxo-amino-acids in PT, while hydrophobic or nonpolar side chains might hinder the process (*15*, *25*). In the design, Ala was placed at alternate positions to Glu to achieve a helical secondary structure suitable for the study.

To assess the structure of the peptide, we performed molecular dynamics (MD) simulations in different solvents: water – an excellent proton donor/acceptor solvent; methanol (MeOH) – a polar protic solvent that is a poor proton donor/acceptor; and chloroform ($CHCl_3$) – an aprotic solvent. The MD results (Fig. 1d and Figure S19) indicated that in MeOH, both the $(EA)_4$ and $(A)_8$ peptides (in their **D**-B-**A** configurations) adopt a mostly α-helical structure. In $CHCl_3$, the $(EA)_4$ peptide possesses less proportion of an *α*-helix structure, whereas the $(A)_8$ peptide has a predominant α-helical structure. In water, the $(A)_8$ peptide still has some percentage of an α-helical structure, but the $(EA)_4$ peptide loses its structure. The results in water are supported by circular dichroism measurements (Figure S23), which could be performed only for the **D**-B-**A** peptides in water due to the solvents' cut-off absorption.

The protonated and deprotonated states of **D** and **A** have different peak positions in both absorption and emission. The ground-state pK_a values of the **D** and **A** UAAs (without Fmoc protection), investigated by UV-Vis spectroscopy using aqueous acid-base titration, were found to be 4.31 and 7.55 for **D** and **A**, respectively (Figure S24). The excited-state pK_a^* values were determined using Förster cycle calculations (*26*) and were found to be 11.12 and -0.32 for Glu-6AQ and Lys-7HC, respectively, thus creating an enormous ΔpK_a^* of 11.4 units between **D** and **A** that serves as the PMF for PT across the bridge. Importantly, using fluorescence measurements while exciting the **D** in its protonated form or the **A** in its deprotonated form allows an immediate understanding of whether an excited-state PT process happened by observing the emissive species of the **D**/**A**. At first, we validated using absorption that the **D** and the **A** are primarily protonated and deprotonated, respectively, in all solvents (Figure S25). Switching to fluorescence measurements, we found that only in water did the **D** and **A** undergo deprotonation and protonation, respectively, while in MeOH and $CHCl_3$, the **D** could not deprotonate, and the **A** could not protonate (Fig. 2a and 2b for the **D** and **A**, respectively). To understand the kinetics associated with the process, we recorded the time-resolved emission spectra (TRES) that were converted into time-resolved area-normalized emission spectra (TRANES). The results revealed a sub-ns deprotonation of the **D** (Fig. 2c-2e) and protonation of the **A** (Fig. 2f-2h), but only in water, meaning that the **D** and **A** UAAs cannot undergo excited-state PT in both MeOH and $CHCl_3$ (the TRES results are in Figures S26 and S27 for the **D** and **A**, respectively).

Two important control experiments were done to exclude the possibility of inter- and intra-molecular PT between the **D** and the **A** in the absence of a bridge. To exclude intermolecular PT, we performed a **D** vs **A** titration in MeOH, and no deprotonation/protonation of **D**/**A** was observed even at high concentrations of **A** (Figure S28). To exclude intramolecular PT without the peptide bridge, we covalently connected the **D** and **A** UAAs (SI section 2.5 and Scheme S5) where no deprotonation/protonation of **D**/**A** was observed in MeOH or $CHCl_3$ (Figure S29 and S30). At this stage, it is essential to note that, while having both the **D** and **A** in the system, the fluorescence measurements are primarily indicative of the **D** and are 'blind' to the **A**. This is due to the overlap in peak positions of the **D** and **A** fluorescence spectra (Fig. 2a and 2b) and the much lower quantum yield of the quinoline **A** with respect to the coumarin **D** (*27-29*).

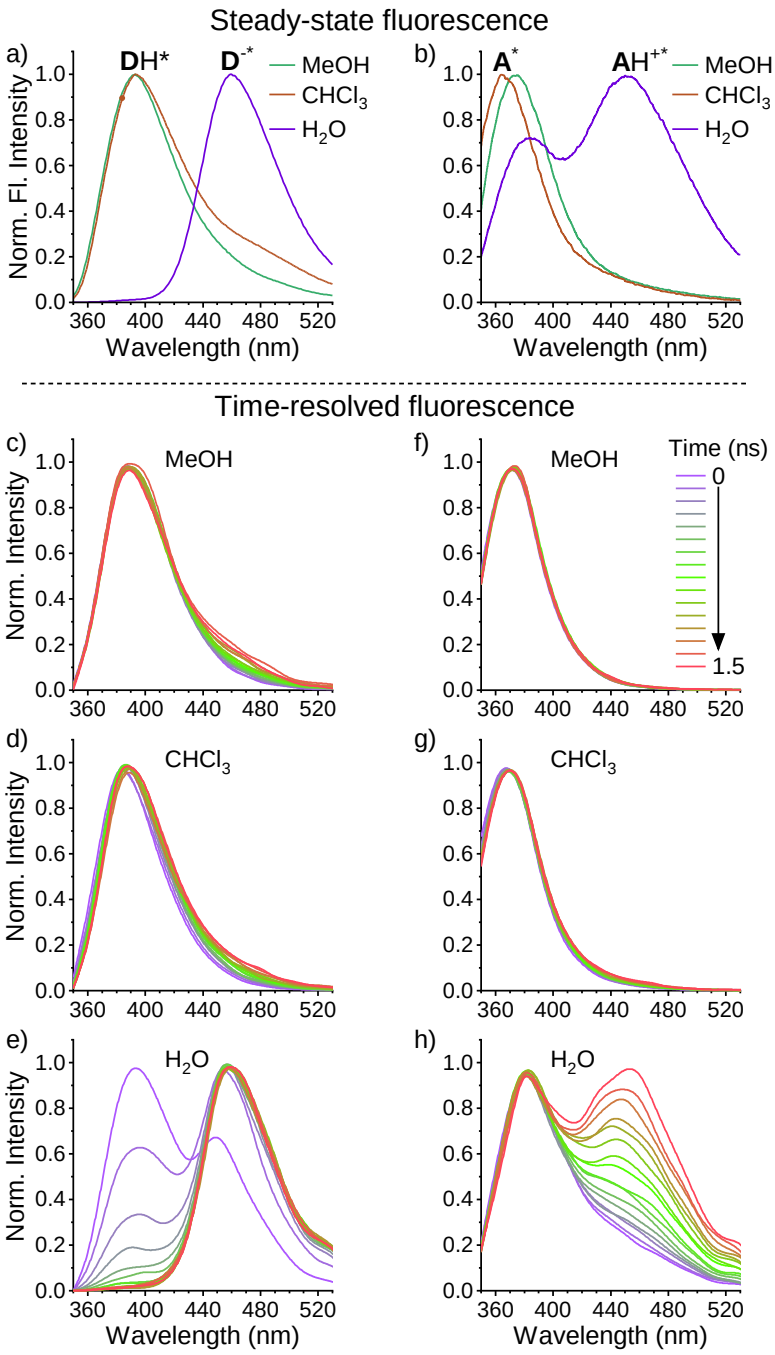

Fig 2: The fluorescence properties of the **D** and **A** UAAs. Normalized steady-state fluorescence spectra for the (a) **D** and (b) **A** UAAs at different solvents. TRANES of the (c-e) **D** and (f-h) **A** UAAs at different solvents.

Next, we followed PT across our two synthesized peptide bridges, $(EA)_4$ and $(A)_8$. To test our hypothesis and the role of the PMF in the PT process, we compared the results of a **D**-B-**A** system having the PMF to a system composed of only **D**-B. As discussed, water is an excellent proton acceptor/donor solvent. Accordingly, a plausible outcome is a fast PT between water and **D**/**A**, with no role of the bridge. However, we found a clear change in the fluorescence spectra even in water but only when having the **D**-B-**A** system (Figure S32), indicating a larger proportion

of the protonated **D**, which will be ascribed to a geminate recombination process (*vide infra*). Nevertheless, the most astonishing results were with MeOH and $CHCl_3$. As discussed, in MeOH, the **D** alone could not deprotonate in the excited-state (Fig. 2a). Still, in the **D**-B-**A** system of both peptide sequences, we could observe the deprotonation of the **D** in the fluorescence spectrum by the emergence of the peak associated with deprotonated **D** (Fig. 3a and 3c). For the $(A)_8$ peptide, only the **D**-B-**A** configuration showed a deprotonated **D** species, while the **D**-B control did not (Fig. 3c), thus indicating the fundamental role of the PMF in driving the PT process for this peptide. On the other hand, for $(EA)_4$, we observed some deprotonation of **D** even in the **D**-B control (Fig. 3a), indicating that the bridge itself, composed of titratable amino acids, can serve as the PMF initiating the PT process. In $CHCl_3$, the fluorescence measurements revealed the formation of deprotonated **D** only in the **D**-B-**A** configuration for the $(EA)_4$ peptide (Fig. 3b), whereas the $(A)_8$ peptide did not show it (Fig. 3d). This finding already highlights the role of the solvent (polar MeOH vs. non-polar $CHCl_3$) and of the peptide's structure in these solvents (see discussion below) in the PT process.

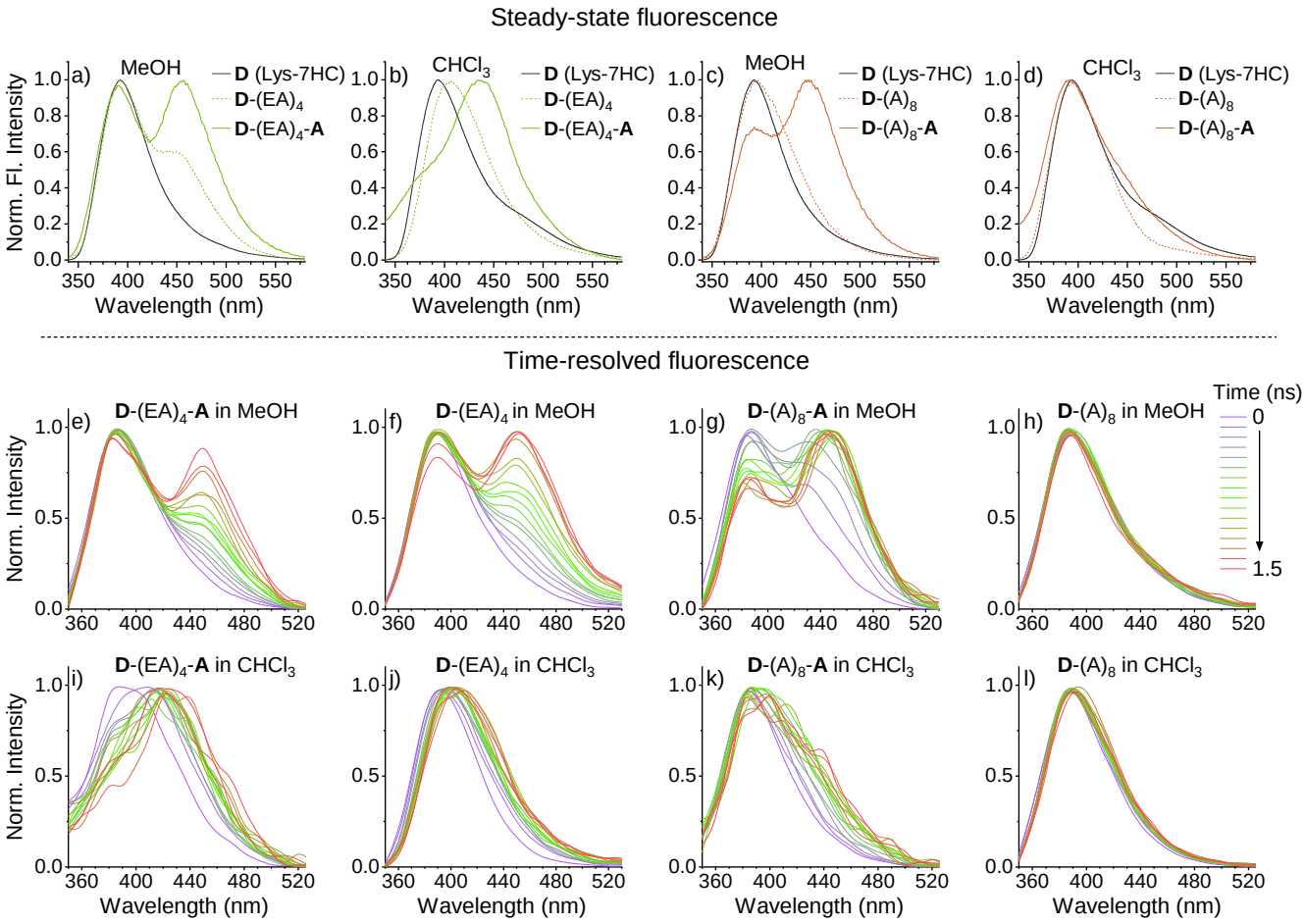

Fig 3: The fluorescence properties of the peptides in **D**-B-**A** and **D**-B configurations. (a-d) Normalized steady-state fluorescence spectra and (e-l) TRANES for the different peptide bridges [$(EA)_4$, and $(A)_8$] in MeOH and $CHCl_3$.

Since the steady-state fluorescence spectra provide only the stationary averaged state of the system, we conducted time-resolved fluorescence measurements. In water, the time-resolved measurements revealed the source for the different emission spectrum of the **D** in the **D**-B-**A** (Figure S33a) configuration compared to just the **D** in water (Figure S33b). They show (Figure

S33) that the difference is not due to a change in the fast PT from the **D**, manifested in the early ps-time scales (Table S2 for the extracted rates), but it results from a geminate proton recombination process from the peptide bridge happening on the nanosecond time scale (further discussion in SI section 8.4). Such differences in the **D** emission in water (**D** vs **D**-B-**A** configuration) highlight that even in water, the large ΔpK_a^* and the established PMF result in a PT across the peptide and not 'just' PT to water. In MeOH (Fig. 3e-h), we observed the excited-state deprotonation of the **D** for both $(EA)_4$ and $(A)_8$ peptides in their **D**-B-**A** configuration (Fig. 3e and 3g, respectively), while the $(EA)_4$ peptide showed the deprotonation of the **D** even in the absence of the **A** (Fig. 3f). In $CHCl_3$ (Fig. 3i-l), we have observed such deprotonation only for the $(EA)_4$ bridge and only for the **D**-B-**A** configuration (Fig. 3i).

From the time-resolved fluorescence measurements, we could directly observe the PT from the **D** and the role of the bridge, solvent, and the presence of the **A** in the deprotonation process of the **D**. However, as discussed, the fluorescence measurements do not provide direct evidence for the protonation of the **A** during the PT process due to the overlap in the **D** and **A** emission spectra and the low quantum efficiency of the **A**. Therefore, we have employed ultrafast transient absorption (TA) spectroscopy in the UV-visible region to observe this process. Here, we used only MeOH as a solvent since the solubility of the samples in $CHCl_3$ was not sufficient to perform TA measurements. At first, to assign the various measured signals to either the protonated or deprotonated states of the **D** or **A**, we measured only the UAAs in their different states (Fig. 4a and 4b for the TA spectra at 100 ps pump-probe delay and Figure S35 at different delays). For the **D** (Fig. 4a), upon deprotonation, we observed a shift in the negative stimulated emission (SE) band from 405 to 465 nm (consistent with the fluorescence spectra of **D**, Fig. 2a) and a change in the positive excited state absorption (ESA) band at 350 nm. For the **A** (Fig. 4b), upon protonation, we observed a red shift in the broad ESA band around 360 nm, a more intense broad SE band from 450 to 500 nm, and a sharper ESA band at 560 nm. Overall, the spectral shapes of the TA spectra from deprotonated **D** and protonated **A** are distinctly different, although the SE peak positions are very close. Since in both **D** and **A**, we observed a strong ESA signal around 330-370 nm masking the ground state bleaching signals, we focused on the discussed SE (at 465 nm) and ESA (at 560 nm) signals to investigate the deprotonation and protonation processes of the **D** and **A**, respectively.

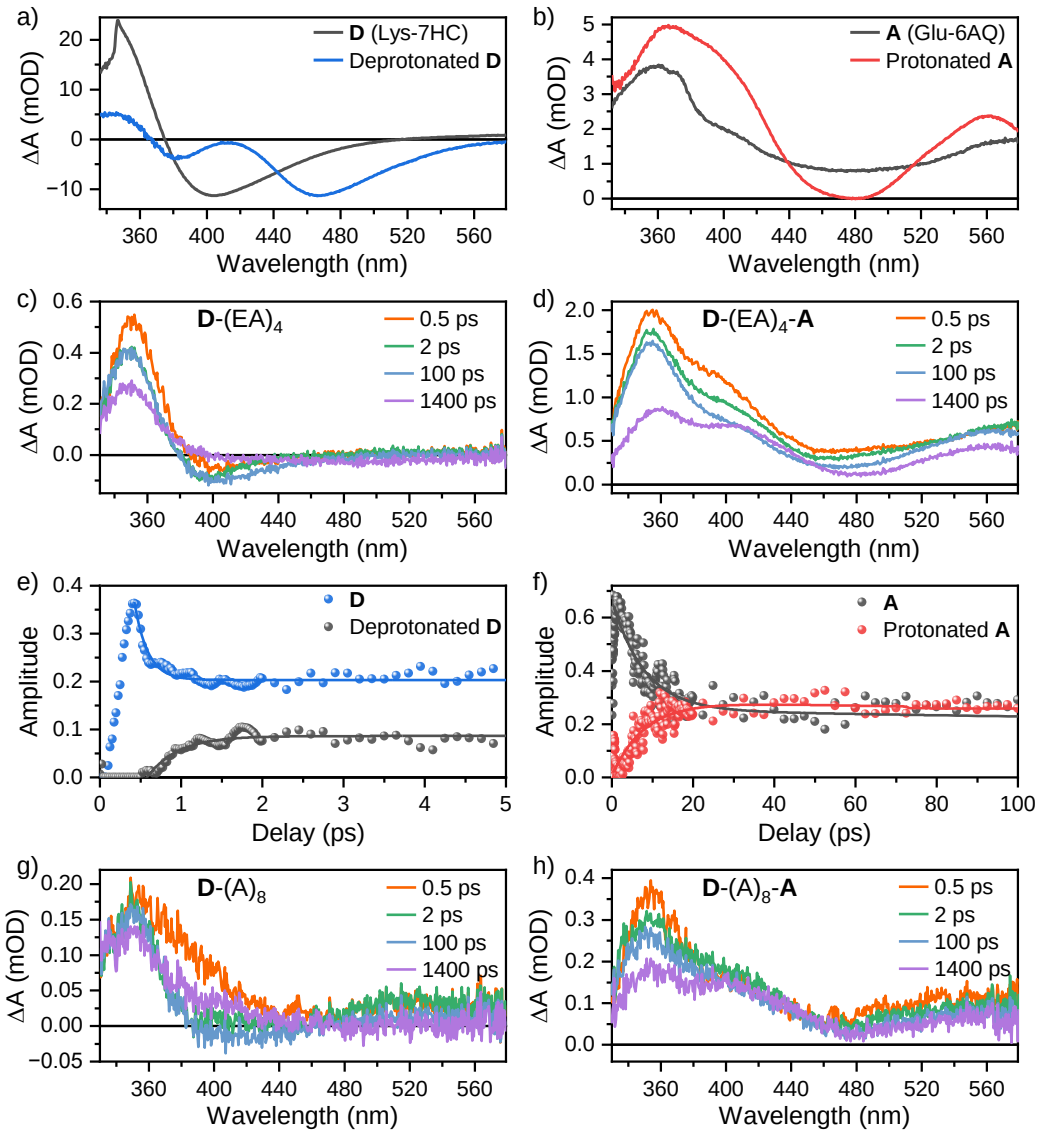

Fig 4: Real-time monitoring of PT using ultrafast TA spectroscopy: TA spectra of (a) **D** and deprotonated **D**, (b) **A** and protonated **A** at 100 ps time delay after excitation at 300 nm. TA spectra of (c) **D**-$(EA)_4$ and (d) **D**-$(EA)_4$-**A** at different time delays after excitation. Kinetics of (e) **D** and deprotonated **D**, (f) **A** and protonated **A** in **D**-$(EA)_4$-**A** peptide. TA spectra of (g) **D**-$(A)_8$ and (h) **D**-$(A)_8$-**A** at different time delays after excitation.

Next, we measured the TA spectra of the $(EA)_4$ peptide following excitation at 300 nm. The TA spectra at different time delays for **D**-$(EA)_4$ and **D**-$(EA)_4$-**A** are shown in Fig. 4c and 4d, respectively. At early delays, **D**-$(EA)_4$ shows a similar pattern as that of the **D**, with a SE signal peaking around 405 nm, whereas **D**-$(EA)_4$-**A** is a superposition of the TA spectra of **D** and **A,** both excited by the 300-nm pump pulse. However, at longer delays, only the **D**-$(EA)_4$-**A** exhibits a broad and prominent dip, reminiscent of a negative signal, around 450-500 nm. Moreover, this is accompanied by a sharper ESA band around 560 nm, present only in the protonated **A** spectra, confirming the PT to the **A**. To extract the timescales of deprotonation of the **D** and protonation of the **A**, we performed evolution-associated spectra analysis of the individual **D**, **A**, deprotonated **D**, and protonated **A** (the fitting data at selected time delays are shown in Figures S36 and S37 and the fitting procedure is explained in the SI)(*30*). Due to the dominance of the **A** signals in the fitting

at longer time scales, the signals of the **D** could be fitted only for very short timescales. The fitting results for the **D**-$(EA)_4$-**A** peptide clearly show that the **D** starts to deprotonate within one picosecond together with a rapid (~20 ps) protonation of the **A** (Fig. 4e and 4f, respectively).

While switching to the TA measurements of the $(A)_8$ peptides (Fig. 4g and 4h for the TA spectra at different time delays for **D**-$(A)_8$ and **D**-$(A)_8$-**A**, respectively), we can make two important observations. The first one is the lack of the ultrafast decay of the 350 nm band for **D**-$(A)_8$ (Fig. 4g), in contrast to the results of **D**-$(EA)_4$ (Fig. 4c). This observation serves as an indication for the lack of the **D** deprotonation in **D**-$(A)_8$, which is in line with our fluorescence measurements. The second observation is that the TA spectra for **D**-$(A)_8$-**A** exhibit a broad dip around 450-500 nm, which is not present in **D**-$(A)_8$, and is highly similar in shape to the one of **D**-$(EA)_4$-**A** (Fig. 4d). As discussed, this signal is attributed to the SE from deprotonated **D** and protonated **A**, which validates the PT from **D** to **A** through the $(A)_8$ peptide bridge. Due to the poor signal-to-noise of the data for the $(A)_8$ peptides (owing to their poor solubility), we could not perform the evolution-associated spectra analysis. Nonetheless, qualitatively, we see similar time scales of the TA decay.

The main remaining question to be answered is: How come the **D**-$(A)_8$-**A** peptide in MeOH supports PT from **D** to **A**, taking into consideration the hydrophobic nature of the Ala side chain? To answer this question, we will refer to the peptides' structure, as estimated using MD. The only structural feature of the $(A)_8$ peptide that can support PT is its polar backbone, which can participate in hydrogen bonding. Accordingly, the estimated α-helical structure of the **D**-$(A)_8$-**A** peptide can result in a pathway for PT from **D** to **A**. However, the observation of PT for the **D**-$(A)_8$-**A** peptide only in MeOH and not in $CHCl_3$, although the peptide adopts an α-helix structure in both solvents (Fig. 1d), suggests that the structure is not enough, and there is a need for the polar MeOH molecule to bridge-in between the polar moieties of the peptide backbone to facilitate PT across the peptide.

Conclusion and outlook

In this research, we introduced a **D**-B-**A** system to induce and probe PT across peptides using UAAs that serve as the light-triggered proton **D** and **A**. By comparing the PT across a peptide containing titratable oxo-amino-acids to a peptide with hydrophobic residues in different solvents we revealed some expected and some surprising findings. The expected one is that titratable amino acids can support PT across a peptide segment. Nevertheless, we further proved that PT across titratable amino acids can occur not only in a polar environment but even in a pure aprotic environment. Using ultrafast measurements, we revealed that the peptide-assisted PT process is happening on the picosecond time scale. In nature, PT across proteins commonly has much slower time scales due to the necessity of maintaining PT directionality, which is usually due to a slower structural change of the protein. In contrast, in our new model system, the large PMF from the excited **D** to **A** dictates directionality, and the PT across the peptide segment can be directly explored. The most surprising finding is that hydrophobic peptides can also support PT while having a PMF, whereas the α-helical structure and the polar environment (solvent) are suggested to be essential. In such conditions, the polar solvent can bridge between the polar backbone of the helix and facilitate PT. While discussing the inner pathways within proteins, the polar environment can consist of polar (non-titratable) residues. For a future outlook, the next immediate step will consist of incorporating these UAAs into proteins, which will allow initiating and visualizing PT pathways within them, a project we are working on nowadays.

Acknowledgments

GC acknowledges financial support by the European Union's NextGenerationEU Programme with the IPHOQS Infrastructure (IR0000016, ID D2B8D520, CUP B53C22001750006) "Integrated Infrastructure Initiative in Photonic and Quantum Sciences". NA acknowledges financial support by UKRI awards, Horizon Europe guarantee scheme grant (number R/185766-11-1): "ProtonsInProteins".

References

1. D. Stock, A. G. W. Leslie, J. E. Walker, Molecular Architecture of the Rotary Motor in ATP Synthase. *Science* **286**, 1700-1705 (1999).
2. T. Elston, H. Wang, G. Oster, Energy transduction in ATP synthase. *Nature* **391**, 510-513 (1998).
3. P. Mitchell, Coupling of Phosphorylation to Electron and Hydrogen Transfer by a Chemi-Osmotic type of Mechanism. *Nature* **191**, 144-148 (1961).
4. A. Mezer, R. Friedman, O. Noivirt, E. Nachliel, M. Gutman, The Mechanism of Proton Transfer between Adjacent Sites Exposed to Water. *J. Phys. Chem. B* **109**, 11379-11388 (2005).
5. A. Burnstine-Townley, S. Mondal, Y. Agam, R. Nandi, N. Amdursky, Light-Modulated Cationic and Anionic Transport across Protein Biopolymers. *Angew. Chem. Int. Ed.* **60**, 24676-24685 (2021).
6. H. Luecke, H.-T. Richter, J. K. Lanyi, Proton Transfer Pathways in Bacteriorhodopsin at 2.3 Angstrom Resolution. *Science* **280**, 1934-1937 (1998).
7. P. Brzezinski, P. Ädelroth, Pathways of Proton Transfer in Cytochrome c Oxidase. *J. Bioenerg. Biomembr.* **30**, 99-107 (1998).
8. J. ter Beek, N. Krause, J. Reimann, P. Lachmann, P. Ädelroth, The Nitric-oxide Reductase from Paracoccus denitrificans Uses a Single Specific Proton Pathway*. *J. Biol. Chem.* **288**, 30626-30635 (2013).
9. C. Tu, M. Qian, J. N. Earnhardt, P. J. Laipis, D. N. Silverman, Properties of Intramolecular Proton Transfer in Carbonic Anhydrase III. *Biophys. J.* **74**, 3182-3189 (1998).
10. S. Yoshikawa, K. Muramoto, K. Shinzawa-Itoh, Proton-Pumping Mechanism of Cytochrome c Oxidase. *Annu. Rev. Biophys.* **40**, 205-223 (2011).
11. B. C. Tripp, J. G. Ferry, A Structure−Function Study of a Proton Transport Pathway in the γ-Class Carbonic Anhydrase from Methanosarcina thermophila. *Biochemistry* **39**, 9232-9240 (2000).
12. H. Ishikita, K. Saito, Proton transfer reactions and hydrogen-bond networks in protein environments. *J. R. Soc. Interface* **11**, 20130518 (2014).
13. A. V. Pisliakov, T. Hino, Y. Shiro, Y. Sugita, Molecular Dynamics Simulations Reveal Proton Transfer Pathways in Cytochrome C-Dependent Nitric Oxide Reductase. *PLOS Computational Biology* **8**, e1002674 (2012).
14. M. Gutman, E. Nachliel, R. Friedman, The dynamics of proton transfer between adjacent sites. *Photochem. Photobiol. Sci.* **5**, 531-537 (2006).
15. A. W. Duster, H. Lin, Tracking Proton Transfer through Titratable Amino Acid Side Chains in Adaptive QM/MM Simulations. *Journal of Chemical Theory and Computation* **15**, 5794-5809 (2019).
16. J. R. Winkler, D. G. Nocera, K. M. Yocom, E. Bordignon, H. B. Gray, Electron-transfer kinetics of pentaammineruthenium(III)(histidine-33)-ferricytochrome c. Measurement of

the rate of intramolecular electron transfer between redox centers separated by 15.ANG. in a protein. *J. Am. Chem. Soc.* **104**, 5798-5800 (1982).
17. C. Shih *et al.*, Tryptophan-Accelerated Electron Flow Through Proteins. *Science* **320**, 1760-1762 (2008).
18. S. L. Mayo, W. R. Ellis, R. J. Crutchley, H. B. Gray, Long-Range Electron Transfer in Heme Proteins. *Science* **233**, 948-952 (1986).
19. E. W. Driscoll, J. R. Hunt, J. M. Dawlaty, Proton Capture Dynamics in Quinoline Photobases: Substituent Effect and Involvement of Triplet States. *J. Phys. Chem. A* **121**, 7099-7107 (2017).
20. J. R. Hunt, J. M. Dawlaty, Photodriven Deprotonation of Alcohols by a Quinoline Photobase. *J. Phys. Chem. A* **122**, 7931-7940 (2018).
21. R. Nandi, N. Amdursky, The Dual Use of the Pyranine (HPTS) Fluorescent Probe: A Ground-State pH Indicator and an Excited-State Proton Transfer Probe. *Acc. Chem. Res.* **55**, 2728-2739 (2022).
22. E. W. Driscoll, J. R. Hunt, J. M. Dawlaty, Photobasicity in quinolines: origin and tunability via the substituents' Hammett parameters. *J. Phys. Chem. Lett.* **7**, 2093-2099 (2016).
23. R. Simkovitch, L. P. da Silva, J. da Silva, D. Huppert, Comparison of the Photoprotolytic Processes of Three 7-Hydroxycoumarins. *Journal of Physical Chemistry B* **120**, 10297-10310 (2016).
24. G. Amoruso, V. C. A. Taylor, M. Duchi, E. Goodband, T. A. A. Oliver, Following Bimolecular Excited-State Proton Transfer between Hydroxycoumarin and Imidazole Derivatives. *J. Phys. Chem. B* **123**, 4745-4756 (2019).
25. E. Herzog, T. Frigato, V. Helms, C. R. D. Lancaster, Energy barriers of proton transfer reactions between amino acid side chain analogs and water from ab initio calculations. *Journal of Computational Chemistry* **27**, 1534-1547 (2006).
26. J. F. Ireland, P. A. H. Wyatt, in *Adv. Phys. Org. Chem.*, V. Gold, Ed. (Academic Press, 1976), vol. 12, pp. 131-221.
27. J. R. Heldt, J. Heldt, M. Stoń, H. A. Diehl, Photophysical properties of 4-alkyl-and 7-alkoxycoumarin derivatives. Absorption and emission spectra, fluorescence quantum yield and decay time. *Spectrochimica Acta Part A: Molecular and Biomolecular Spectroscopy* **51**, 1549-1563 (1995).
28. S. G. Schulman, K. Abate, P. J. Kovi, A. C. Capomacchia, D. Jackman, Photoluminescence of 6- and 7-aminoquinolines. *Anal. Chim. Acta* **65**, 59-67 (1973).
29. S. G. Schulman, L. B. Sanders, Fluorescence and phosphorescence of 5- and 8-aminoquinoline. *Anal. Chim. Acta* **56**, 83-89 (1971).
30. J. J. Snellenburg, S. Laptenok, R. Seger, K. M. Mullen, I. H. M. van Stokkum, Glotaran: A Java-Based Graphical User Interface for the R Package TIMP. *Journal of Statistical Software* **49**, 1 - 22 (2012).